Red blood cell lingering modulates hematocrit distribution in the microcirculation

Yazdan Rashidi[1,*], Greta Simionato[1,2], Qi Zhou[3], Thomas John[1], Alexander Kihm[1], Mohammed Bendaoud[1,4,5], Timm Krüger[3], Miguel O. Bernabeu[6], Lars Kaestner[1,7], Matthias W. Laschke[2], Michael D. Menger[2], Christian Wagner[1,8], and Alexis Darras[1,*]

[1]Experimental Physics, Saarland University, 66123 Saarbruecken, Germany
[2]Institute for Clinical and Experimental Surgery, Saarland University, 66421 Homburg, Germany
[3]School of Engineering, Institute for Multiscale Thermofluids, University of Edinburgh, Edinburgh EH9 3FD, United Kingdom
[4]Université Grenoble Alpes, CNRS, LIPhy, F-38000 Grenoble, France
[5]LaMCScI, Faculty of Sciences, Mohammed V University of Rabat, Rabat 1014, Morocco
[6]Centre for Medical Informatics, Usher Institute, University of Edinburgh, Edinburgh EH16 4UX, United Kingdom
[7]Theoretical Medicine and Biosciences, Saarland University, 66421 Homburg, Germany
[8]Physics and Materials Science Research Unit, University of Luxembourg, L-1511 Luxembourg, Luxembourg
[*]Correspondence: yazdan.rashidi@uni-saarland.de, alexis.darras@uni-saarland.de

August 16, 2022

Abstract

The distribution of red blood cells (RBCs) in the microcirculation determines the oxygen delivery and solute transport to tissues. It is known since the last century that RBCs partition at bifurcations disproportionately to the fractional blood flow rate, leading to heterogeneity of the hematocrit (i.e. volume fraction of RBCs in blood) in microvessels. Usually, downstream of a microvascular bifurcation, the vessel branch with a higher fraction of blood flow receives an even higher fraction of RBC flux. However, both temporal and time-average deviations from this phase-separation law have been observed in recent works. Here, we quantify how the microscopic behavior of RBCs lingering (i.e. RBCs temporarily residing near the bifurcation apex due to diminishing velocity) influences their partitioning, through combined in vivo experiments and in silico simulations. We developed an approach to quantify the cell lingering at highly-confined capillary-level bifurcations and demonstrate that it correlates with deviations of the phase-separation process from established empirical predictions by Pries *et al.* Furthermore, we shed light on how the bifurcation geometry and cell mechanical property can affect the lingering behavior of RBCs, e.g. rigid cells tend to linger less strongly than softer ones. Taken together, RBC lingering is an important mechanism that should be considered when studying how the vascular networks are altered under pathological conditions (e.g. thrombosis, aneurysm) or how abnormal RBC rigidity in diseases such as malaria and sicke-cell disease could hinder the microcirculatory blood flow.

Introduction

Partitioning of red blood cells (RBCs) through bifurcations of blood vessels determines how the oxygen is delivered to organs. Early works from Zweifach-Fung and Fahraeus showed that it's far from being a

trivial phenomenon [1, 2, 3], and since then it has been an area of intensive research [4, 5, 6, 7, 8]. More accurately, vessels with a higher flow rate tend to collect an even higher proportion of RBCs. This fact is known as the Zweifach-Fung effect and leads to inhomogeneity in the hematocrit of various vessels [1]. Although Pries *et al.* developed an empirical model, which reproduces this average behavior [9, 10, 11, 12]. Various experiments, both in vitro and in vivo, along numerical simulations, kept showing that deviations are observed from this model for various reasons [6, 7, 13]. In particular, it has been shown that bifurcations in the smallest vessels of the microvascular network tend to deviate from this empirical model prediction [14, 15, 16, 17]. On the other hand, recent numerical simulations and in vivo experiments highlighted that RBCs tend to linger at the apex of bifurcations, modifying the dynamics of cells entering a single vessel and their characteristic inter-distance [18, 15, 19]. In the present study, we analyzed systematically how the lingering of RBCs influence their partitioning in the microcirculation, through in vivo experiments and numerical simulations. We show that the deviations from the Pries model are directly correlated with the normalized average duration of cells lingering. This asymmetric drive can either reinforce or revert the Zweifach-Fung effect. Moreover, RBCs exhibit large deformations while lingering. We further explored numerically how rigidified cells differ from healthy ones in their lingering and partitioning. Our results demonstrate and quantify the lingering as a source of deviation from the Zweifach-Fung partitioning, and provides a new explanation of how pathologically ridified cells can impair the partitioning of RBCs in the microcirculation [20, 21, 22, 23, 24, 25].

Materials and Methods

In Vivo Experiments

Permissions

Experiments were performed in Syrian golden hamsters according to the German legislation on protection of animals and were approved by the local governmental animal protection committee (permission number: 25/2018). Hamsters were maintained on a standard 12/12 h day/night cycle and water and food were provided ad libitum. Detailed methods are described below for each type of investigation.

Animal preparation and microscopy

Hamsters with an age of 5 to 7 weeks, weighing 55 to 70 g, were used for the implantation of a dorsal skinfold chamber [26]. The surgery was performed under deep anesthesia (150 mg/kg ketamin (Serumwerke Bernburg AG)/ 0.25 mg/kg domitor (Orion Pharma) i.p.), with intraoperative pain medication by carprofen (10 mg/kg, Zoetis, s.c.). A previously described protocol [26] was followed. Briefly, the back of the hamsters was shaved and a titanium chamber consisting of two frames was implanted on the lifted dorsal skinfold. On the frame with a circular observation window (diameter of 10 mm) the cutis, subcutis and retractor muscle were removed to expose the striated skin muscle for later observation of the microcirculation. The window was closed with a cover glass that was fixed with a snap ring. An implanted dorsal skinfold chamber is depicted in Fig. 1(a). Animals were allowed to recover for 72 hours after the procedure.

Hamsters were anesthetized as described above prior to intravital microscopy. A volume of 100 µL of the fluorescent plasma marker fluorescein isothiocyanate(FITC)-labeled (5%, 150 kDa, Sigma-Aldrich) was injected retro-orbitally and the animals were fixed on a plexiglas stage, as illustrated in Fig. 1(b). Several capillary bifurcations in different areas of the chamber window were chosen for epifluorescence microscopy (Axio Examiner A1, Zeiss). FITC-labeled dextran was excited with a 480 nm LED (Colibri 7, Zeiss) and image contrast was additionally enhanced by simultaneously using transmitted blue light that is absorbed by hemoglobin, making RBCs appear darker. Imaging was performed with 20x (LD A-Plan, NA=0.35, Zeiss), 50x (LD EC Epiplan-Neofluar, NA=0.55, Zeiss) or 100x (LD C Epiplan-Neofluar 100x, NA=0.75, Zeiss) long-distance objectives. Video acquisition was carried out with a digital camera (Hamamatsu Orca Flash 4.0, C13440) using the software ZEN 3.1 Blue (Zeiss). For each video, 2000 frames were recorded at different rates according to flow velocity (100 to 170 Hz). A 2x2 binning was applied during acquisition. An example of an obtained image is given in Fig. 1(c).

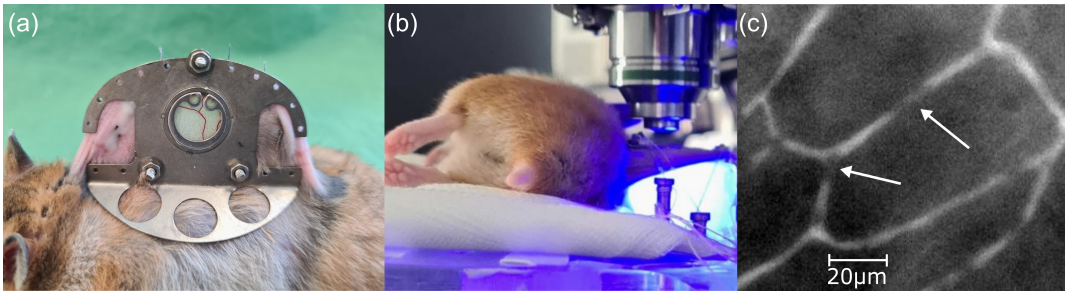

Figure 1: **Experimental Methods**: (a) Dorsal skinfold chamber implanted on the back of a hamster. (b) Anesthetized hamster placed underneath the objective of an epifluorescence microscope. (c) Example of a microvascular network imaged by fluorescence microscopy. The dyed plasma appears bright, while RBCs in the capillaries and the surrounding tissues are dark (arrows).

Image analysis and lingering quantification

Despite the animal being fixed on the plexiglas stage, its breathing and/or muscles movement caused slight translations of the microscopic field of view in the image sequence. In order to determine the motion of the RBCs in the vessels, we first correct those translations by translating each image by the maximum of its 2D-correlation with the first image in the sequence. This process creates a movie where the vessels and surrounding tissues are still (see Supp. Fig.S1(b)). A Gaussian filter (with standard deviation of 2 pixels) is then applied to despeckel the images, and a mask is drawn around the vessels. The creation of this mask is facilitated by also considering the image showing the standard deviation of each pixel intensity along time, which is higher in the vessels with transient (dark) RBCs and offers a guide to the eye for the mask drawing (see Supp. Fig.S1(c)). The diameters D of the various vessels are computed as twice the average distance from the skeleton pixels of the masks to the border of the vessels, using standard Matlab functions bwmorph and bwdist (see Supp. Fig.S1(c)). The image series is then inverted and binarized inside the mask area with a threshold based on a user-defined fraction of the Otsu threshold [27]. Otsu thresholding method was used because the average intensity of images is usually slightly flickering. However, the automated threshold algorithm overestimated the threshold required to detect the whole RBCs, hence we implemented a user-defined ratio to adjust it (see Supp. Fig.S1(d)).

A tracking algorithm [28] was then used to determine the velocity of the detected RBCs. The variations of light intensity along the vessels, in conjunction with the collisions and transient aggregations of RBCs, didn't allow us to reliably follow all RBCs along their entire trajectories. However, as we focused on bifurcations where the mother vessel (M) and the two daughter vessels have a hematocrit low enough to distinct single RBCs, this tracking allowed us to extract the spatial distribution of the RBC velocity (i.e. we performed Particle Tracking Velocimetry), on which we performed our further analyses. In this manuscript, we will refer to both daughter vessels as main and secondary daughter vessels, respectively abbreviated MD and SD. The MD is identified as the daughter vessel with the highest total blood flow rate.

More accurately, in order to detect lingering of RBCs, we applied a method similar to previous investigations [19]: We defined a circle with a diameter of 6 μm (i.e. one cell's main diameter) around the bifurcation apex (Fig. 3(a)). The cells were considered to linger if they were in this circle and had a velocity lower than the local minimum detected in the PDF of the velocity (Fig. 3(b)). The velocity PDF displayed in Fig. 3(b) was obtained when considering the mother vessel and the bifurcation area.

Numerical simulations

Complementary simulations for the RBC flow in similar capillary bifurcations were run with *HemeLB* (`https://github.com/hemelb-codes/hemelb`) using the immersed-boundary-lattice-Boltzmann method (IB-LBM, see Supplementary Material) following our previous approach [14]. First, three-dimensional (3D) luminal surface models were reconstructed from binary masks of the capillary bifurcations using open-source software *PolNet* [29], assuming circular cross-sections of varying diameter along each vessel. Then the flow domain enclosed by the luminal surface was uniformly discretised into cubic lattices

of fine voxel size $\Delta x = 0.25\ \mu m$, aimed at resolving cell dynamics with high resolution at the bifurcation apex. To initialize the simulation, inflow/outflow boundary conditions based on experiment-measured volume flow rates were imposed at the end of the mother vessel (M) and the main daughter branch (MD, the daughter branch with higher flow rate) of each bifurcation, and a reference pressure for the secondary daughter branch (SD, the daughter branch with lower flow rate). No-slip boundary conditions were imposed at the vessel wall. The simulation time step length was $\Delta t = 1.04 \times 10^{-6} s$.

The simulation for each bifurcation was initialised with (RBC-free) plasma flow. Once the plasma flow converged, RBCs were randomly inserted from the M vessel through a cylindrical flow inlet with constant feeding hematocrit (H_{F}) as measured from experiments. When RBCs reached the end of MD or SD, they were removed from the simulation domain. Each RBC was modeled as a cytosol-filled capsule with an isotropic and hyperelastic membrane consisting of 5120 triangular facets. The mechanical properties of the RBCs were governed by elastic moduli governing different energy contributions, such as shearing and bending of the membrane. The cytosol was treated as a Newtonian fluid with the same viscosity as the suspending medium, *i.e.* blood plasma. The viscosity of the RBC membrane itself was not considered. Two different RBC sizes ($D_{\mathrm{rbc}} = 6\ \mu m$ and $8\ \mu m$) and membrane rigidity levels (stain modulus $\kappa_s = 5 \times 10^{-6}, 5 \times 10^{-5} N/m$ for representing a normal and a hardened cell) were considered.

Results and Discussion

Determination of flow rates and expected Zweifach-Fung partitioning

In order to determine how the lingering of RBCs influence their partitioning, we used the model of Pries *et al.* for the Zweifach-Fung effect [11] as a baseline. For this purpose, we first determined the blood flow rate Q in each vessel. Since the vessels were smaller than the main radius of the RBCs, we assumed a plug flow. We also assumed that the difference between the tube and discharge hematocrits was negligible in our observations. The flow rates within all bifurcation segments were therefore initially assessed from the velocities (V) and diameter (D) measurements of the individual segments

$$\langle \mathrm{Q} \rangle = \langle \mathrm{V} \rangle \pi \left(\frac{D}{2} \right)^2, \tag{1}$$

similarly to previous works [30, 31, 19]. However, volume conservation implies that the total flow rate from the mother vessel Q_M is divided into the daughter branches $Q_M = Q_{MD} + Q_{SD}$. The subscripts MD and SD refer to the Main Daughter and Secondary Daughter, respectively. To obey this conservation law and minimize experimental errors, values obtained from Eq.(1) were corrected by using the normalization described by Pries *et al.* in previous similar measurements [30]. Similarly, the measured erythrocyte flow rates $E_i = H_i Q_i$, H_i being the local hematocrit, were also corrected to obey $E_M = E_{MD} + E_{SD}$. The empirical law for the Zweifach-Fung effect developed by Pries *et al.*[30, 10, 11] describes the relation between fractional blood flow, FQ_b, and the fractional erythrocyte flux, FQ_e, in the microvascular bifurcation. The fractional blood flow FQ_b for both daughter vessels were calculated by dividing the flow rate Q in the respective daughter by the flow rate in the mother vessel. The fractional erythrocyte flow rate FQ_e the ratio of the corrected erythrocytes flow rates, e.g. E_{MD}/E_M for the main daughter. With these definitions, the model from Pries *et al.*[30, 10, 11] states

$$\mathrm{logit}(FQe) = A + B\ \mathrm{logit}\left(\frac{FQb - X_0}{1 - 2X_0} \right), \tag{2}$$

where $\mathrm{logit}(x) = \ln\left(\frac{x}{1-x} \right)$ and A, B, X_0 are related to the geometry of the bifurcation and the hematocrit in the mother vessel

$$A_{MD} = -13.29\ \frac{D_{MD}^2/D_{SD}^2 - 1}{D_{MD}^2/D_{SD}^2 + 1}(1-H_M)/D_M,\ A_{SD} = -A_{MD},\ B = 1+6.98\left(\frac{1-H_M}{D_M} \right),\ X_0 = 0.964\left(\frac{1-H_M}{D_M} \right), \tag{3}$$

where H refers to the measured hematocrit, assessed as the average area fraction of RBC in the mask during the experiment [10, 11]. The subscripts indicate in which vessel the quantity is considered.

Lingering and partitioning

Global description

Experiments Figure 2(a, b, c) shows characteristic bifurcations where all the required parameters could be extracted from the image sequences. We calculated the predictions of Eq.(2) for each available bifurcation, and defined the deviations from the model as $\delta ZF = |\Delta FQ_e(EX) - \Delta FQ_e(ZF)|$. We noted $\Delta FQ_e = FQ_{e(MD)} - FQ_{e(SD)}$ the difference of fractional erythrocytes flow rate, and the expressions EX and ZF are respectively referring to the experimental result and the prediction from Eq.(2). The total blood flow rate FQ_b is given by the experimental measurements, and the predicted fractional erythrocyte flow rate $FQ_e(ZF)$ is computed through Eq.(2) (see Fig. 4(a)).

In order to quantify the lingering of the RBCs in each bifurcation, we first determined the average duration of the lingering events $\langle\tau\rangle$. The total lingering time was considered as the sum of the duration of all detected lingering events. We then determined the ratio of this total lingering time to the number of the RBCs as the characteristic lingering time $\langle\tau\rangle$. Since this time is highly correlated with the flow rate and the transit time of a RBC through the bifurcation (i.e. the red circle defined in Fig. 3(a)), we normalized it by $t_s = R/\langle V_M\rangle$. The radius $R = 3\,\text{um}$ is the radius of the red circle defined in Fig. 3(a) and V_M the average velocity in the mother vessel. The time t_s is then a characteristic advection time that a cell would need to go through the lingering detection area. We defined the ratio of these two characteristic times as $Pe_\lambda = \langle\tau\rangle/t_s$. The ratio Pe_λ defines the equivalent of a Peclet number, since it compares two characteristic times of different transport modes in the bifurcation (lingering and advection). As shown in Fig. 4(c), the deviation δZF from the Zweifach-Fung prediction Eq.(2) strongly correlates linear with Pe_λ (Pearson correlation coefficient $r = 0.811$, with a p-value of $p = 0.007$).

Interestingly, we observed in some case that the deviation from the Zweifach-Fung effect caused by the lingering can revert the partitioning. Indeed, in the case of the (red) characteristic bifurcation highlighted in Figure 2(a), the main daughter (with the highest FQ_b) is also the daughter with the lowest FQ_e. This is often referred to in the literature as reversed partitioning [6, 7, 13]. In our data, we only observed such reverse partitioning for the highest $Pe_\lambda \approx 1.75$.

Simulations The three characteristic bifurcations observed in experiments were also simulated under equivalent flow conditions and RBC volume fractions. The phenomenon of RBC lingering was reproduced (Fig. 2$(d-f)$). To quantify the lingering behavior, the same routine as stated in section. **Image analysis and lingering quantification** was applied to analyze the simulation data.

In line with the experimental particle tracking velocimetry (PTV) measurements, the cell velocities diminished as the RBCs approached the bifurcation apex (Fig. 3(c)). After entering one of the daughter branches (MD or SD), the RBCs accelerated and their instantaneous velocity increased. These patterns were well captured by the velocity PDFs compiled for the individual vessel branches (Fig. 3(d)). Quantification of lingering events based on the RBC velocities revealed that the percentages of lingering cells for the three bifurcations were 48%, 84% and 32%, respectively. For hardened RBCs with a membrane strain modulus ten times as large, the ratios become 31%, 68% and 35%.

The correlation between the lingering intensity of RBCs and their partitioning at the bifurcations, namely δZF and Pe_λ, were evaluated similarly as for the experimental data. A strong association was found, indicating a linear increase of δZF against Pe_λ (Pearson-r correlation coefficient 0.93, $p < 0.01$). Nevertheless, the absolute magnitude of δZF and Pe_λ were substantially smaller (but in a proportional manner) than their experimental counterpart in Fig. 2(e). This discrepancy may be arises from simulation configurations that are different from in vivo experiments, *e.g.* the absence of endothelial surface layer (ESL, with a thickness of roughly 0.4-0.5 μm) and RBC glycocalyx in the numerical model. In any case, the correlation between the lingering Péclet number Pe_λ and the deviation from the Pries model was qualitatively similar in the experiment and the simulation.

Lingering asymmetry in experiments

For more insight into how the lingering behavior could modify RBC partitioning at the bifurcation, we further examined its symmetry between the two daughter branches. Indeed, as can be seen from Supplementary Movie 1, the RBCs tend to enter the lower daughter branch (MD) almost only if there is another cell already lingering at the bifurcation apex. Due to cell collisions at the apex, it was not possible to precisely determine the proportion of lingering cells entering each daughter

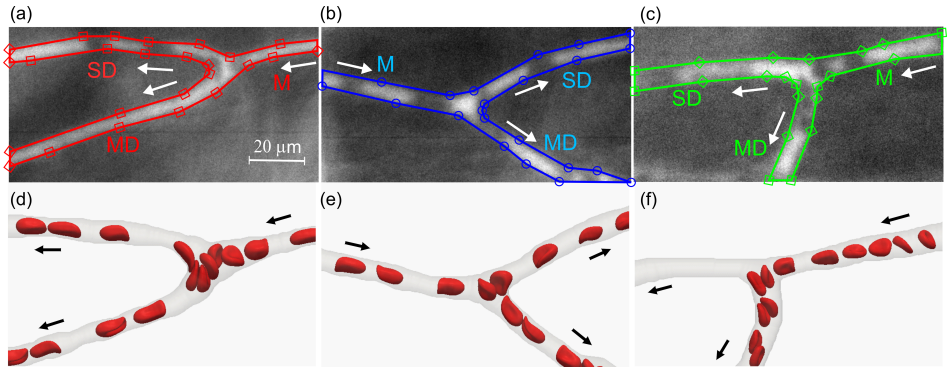

Figure 2: **Representative bifurcations**: $(a), (b), (c)$ The mother vessel (M), the main daughter (MD) and secondary daughter (SD) are annotated and arrows indicates the flow direction. The plasma was stained with fluorescent dye, which is bright in the images. Dark areas in the vessels are RBCs. The border of the masks used to analyze the bifurcations are depicted in colors. Consistent colors are used for these bifurcations throughout the whole manuscript. $(d), (e), (f)$ Simulated RBC flow in reconstructed bifurcations (resp. $(a), (b), (c)$), as characterized experimentally.

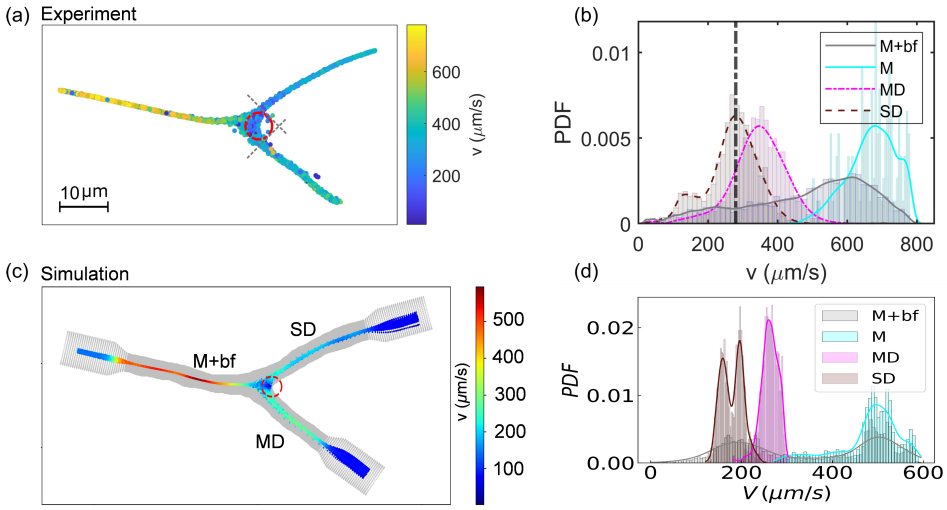

Figure 3: **RBC velocity in experiments and simulations.** (a) Spatial distribution of velocities obtained through particle tracking for experimental data. Lingering is considered to occur if a cell is inside the red circle (6 µm) with a velocity lower than the threshold velocity, determined as a local minimum in the probability density function (PDF) of the velocity obtained in the mother vessel and the bifurcation area (M+bf), as shown in panel (b). For comparison, panel (b) also shows the velocity PDF obtained in both daughter branches (main and secondary daughter vessels, respectively MD and SD). (c) Corresponding color map of RBCs velocities measured along the trajectories of cells for simulation data. (d) PDF of RBC velocities measured from different vessel segments. The symbol M stands for the mother vessel.

merely by analyzing their trajectories. Therefore, we turned to evaluate which cells detected were lingering by monitoring RBCs in a thin mask extracted from the daughter (Fig. 5(a)) and checking if there was a lingering event with a time t_a earlier at the bifurcation (also monitored in a thin mask), where t_a accounts for the average advection time of the cells between the bifurcation and the mask in the daughter. This advection time was determined by calculating the convolution of the temporal hematocrit in the daughter mask and that in the bifurcation mask (see Supp. Fig.S2(b)). We realised that when performing such sorting, some lingering events at the bifurcation were not associated to any advected cell in the daughters. Indeed, the advection time of each cell can vary slightly, depending on its interactions with other cells near the bifurcation apex. After a time translation by t_a, the cell transits in the bifurcation can then be temporally located close to the lingering event, but not

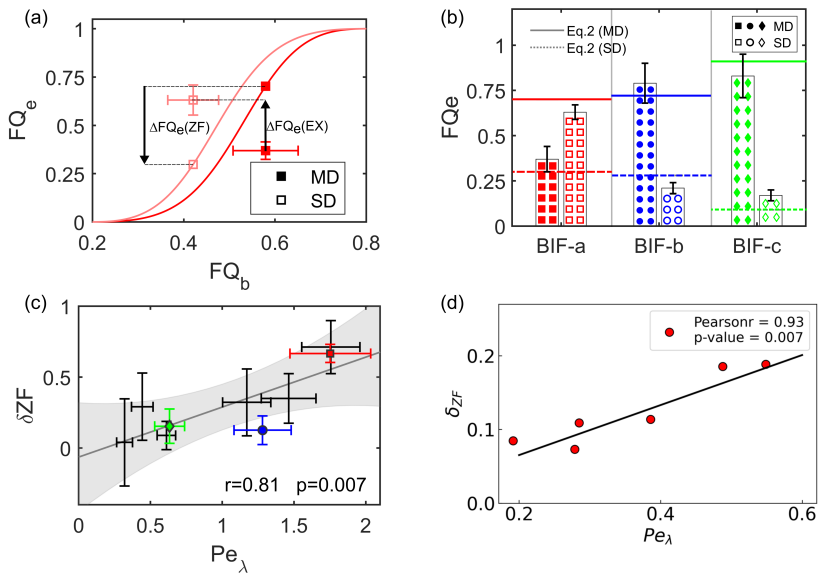

Figure 4: **Experimental and numerical results on partitioning.** (a) Comparison of experimental results of RBC fluxes against the empirical model (for the bifurcation depicted in Fig.2(a)). The axes FQ_e and FQ_b are the fractional RBC flux and fractional blood flow, respectively. We calculated the deviation with Zweifach-Fung prediction δZF as the absolute difference of the experimental result with the prediction of empirical model. (b) Visualisation of the Fractional erythrocyte flow rates FQ_e. Bars are experimental results and lines are predictions from Eq.(2). The data are shown for the characteristic bifurcations in Fig. 2(a, b, c), with consistent colors and symbols. Dashed lines and hollow symbols refer to the secondary daughter vessel (with the lower flow rate). One can then see an inversion of the Zweifach-Fung effect for the first (red) bifurcation. (c) Experimental deviation δZF from Eq.(2) as a function of the lingering Péclet number Pe_λ. Points are experimental data, the solid line is linear regression fitting of the data points, and the shaded area is the 95% confidence interval prediction from the fit. All data gathered during this study (including, but not limited to, the bifurcations in Fig. 2(a, b, c)) are included in this graph. The Pearson-r correlation coefficient is 0.81, with a p-value of 0.007. (d) Correlation between δZF and Pe_λ for simulation data. The circular dots are simulation data and the solid line is linear regression fitting of the data points. The Pearson-r correlation coefficient is 0.93, with a p-value of 0.007.

exactly inside. For this reason, and in order to achieve a more accurate characterization, we measured the proximity time t_i between the closest lingering event and the transit time (detection time in the daughter minus t_a) of each red blood cell. Results are depicted in Fig. 5. Cells with a proximity time $t_i = 0$ can then be detected as lingering. We defined $dp_\tau = |p_{SD} - p_{MD}|$ as the difference between the proportion of lingering cells in both daughter branches. Note that cells with a small proximity time t_i might also have been lingering, or might have interacted with another cell lingering at the apex. We used the difference between the first two points of the CDF of t_i as errorbars for dp_τ (see Fig. 5(c)).

As can be seen in Fig. 5($d - f$), the proximity time t_i and the proportion of cells identified as lingering were not always identical for both daughters. Furthermore, for in vivo conditions, as highlighted in Fig. 5(c), the asymmetry in the proportion of lingering cells could correlate with the Pe_λ. However, such correlation was not observed in the numerical simulations.

Origin of Lingering in experiments

In order to understand what causes the cells to linger, we identified geometrical features of the bifurcations correlating with the lingering Péclet number Pe_λ. Due to the definition of the lingering events as a significant reduction of the RBC velocity in the bifurcation, it is likely that cells linger at the stagnation point, i.e. the point where the local plasma velocity vanishes. At this position, the cells will also experience a negligible drag-force, therefore not pushing the cell towards any daughter vessel. The position of the stagnation point, which is also the intersection of the bifurcation's wall and the

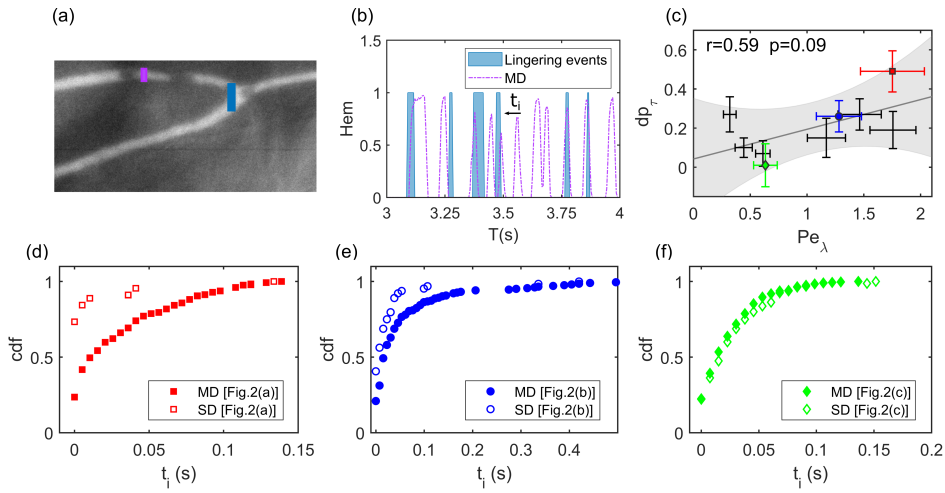

Figure 5: **Asymmetry in Lingering**:(a) Example of mask set used to determine the proximity time t_i of RBCs transit with lingering events. The (blue) mask in the bifurcation is used to determine the average advection time of the cells to the (magenta) mask in the daughter vessel via convolution of the hematocrit in both masks (see main text). (b) Extraction of the proximity time t_i of each cell. The hematocrit variation along time, extracted from the daughter's mask, is first translated by the average advection time t_a (see Supp. Fig.S2). Then, for each peak of this hematocrit along time, a proximity time t_i is obtained as the temporal distance from the closest lingering event. This process is performed independently for the two daughters. (c) The differences dP_τ in proportion of lingering cells (difference in cdf at $t_i = 0$) is significantly correlated with Pe_λ. (d, e, f) Cumulative Density Function (CDF) of the proximity time to lingering events for both daughters of the characteristic bifurcations. When a significant difference is observed in the experiments, higher proportion of lingering cells (and a closer proximity with lingering events) is usually obtained in the secondary daughter.

flow divider plane, depends on the fractional flow rate of the daughter branches [32]. The distance of the stagnation point from the center line L_s, which is depicted in the Fig. 6(a), can be approximated through

$$\frac{\mathrm{FQ_{b(MD)}}}{\mathrm{Q_{b(SD)}}} = \frac{1 + \frac{2}{\pi}\arcsin(\frac{L_s}{R_M}) + \frac{2L_s}{\pi R_M^2}\sqrt{R_M^2 - L_s^2}}{1 - \frac{2}{\pi}\arcsin(\frac{L_s}{R_M}) - \frac{2L_s}{\pi R_M^2}\sqrt{R_M^2 - L_s^2}}, \tag{4}$$

where the R_M is the radius of the mother branch (see Supplemental Material for further justification). For the situations where numerical simulations were compared to the experimental data, location of the stagnation point determined this way were located within one pixel of distance from the position indicated by the streamlines (See Supplemental Fig. S4). This approximation can then be considered to be consistent with the available numerical data.

In order to find the curvature of each bifurcation, we used the best-fit circle function at the stagnation point (Supp. Fig. S4 illustrates this process). We defined the curvature of the bifurcation as the inverse of the radius of the locally fitting circle and showed that it correlates with Pe_λ ($r = 0.58$ and $p = 0.09$) (see Fig. 6(b)). Interestingly, when testing further possible correlations, we found that the lingering Péclet number Pe_λ also correlates with the ratio of the flow rates between the secondary and main daughters Q_{SD}/Q_{MD} (Fig. 6(c)). Since this parameter determines the distance L_S between the apex of the bifurcation and the stagnation point through Eq.(4), this parameter L_S also correlates with Pe_λ. Furthermore, the bifurcations where the stagnation point is further from the apex generally have a lower curvature at the stagnation point, as shown by Fig. 6(e). We therefore concluded that the flow rate ratio determines where the cells can linger, while the curvature of the endothelial layer at this lingering position determines the intensity of the lingering. The lingering Péclet number is then determined by an interplay between global parameters of the bifurcation (Q_{SD}/Q_{MD}) and local geometries of the endothelial layer (the curvature at the stagnation point, ζ). When it comes to the experimental correlations, the fact that a lower p-value is found between Pe_λ and ζ than Pe_λ and

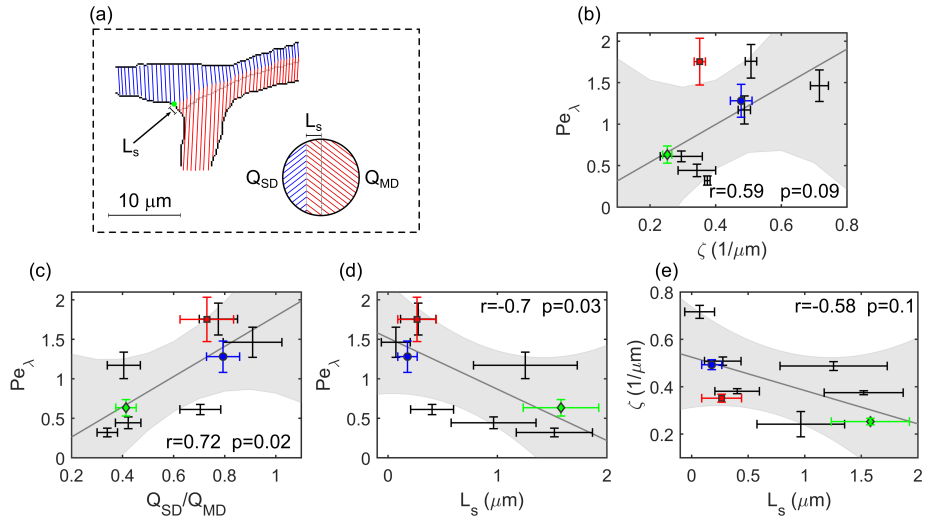

Figure 6: **Potential origin of Lingering**: (a) Scheme highlighting the stagnation point. Flow in the mother branch splits into flows Q_{MD} and Q_{SD} in the MD and SD branches, respectively. The stagnation point is the green point. Its distance at the apex L_s is highlighted with the arrow and scale symbol. (b) Correlation of the lingering Péclet number Pe_λ with the curvature of the bifurcation, at the stagnation point. (c) Correlation between Pe_λ and the flow rate ratio between the secondary and main daughters Q_{SD}/Q_{MD}. (d) Correlation between Pe_λ and the distance between the stagnation point and the apex of the bifurcation L_S. (e) Correlation between L_S and the curvature at the stagnation point ζ. Points are experimental data, the solid line is linear regression fitting of the data points, and the shaded area is the 95% confidence interval prediction from the fit.

Q_{SD}/Q_{MD} likely arises from the fact that the determination of ζ also determines on the approximation for L_S and then the measurement of Q_{SD}/Q_{MD}. The error propagation on these successive quantities then decreased artificially the correlation between Pe_λ and the successively determined parameters L_S and ζ.

Further geometrical parameters, which didn't present a significant correlation with Pe_λ, are shown in Supplementray Materials (see Supp. Fig. S5).

Effect of Cell Rigidity and Hematocrit in simulations

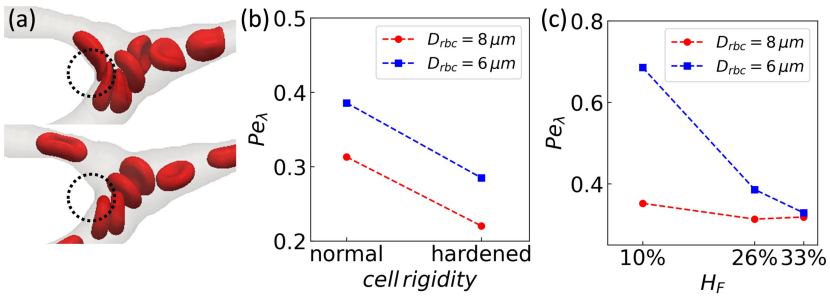

Figure 7: **Effect of cell rigidity and feeding hematocrit on the lingering of RBCs.** (a) Steric repulsion from bifurcation apex for (top) normal and (bottom) hardened RBCs. (b) Pe_λ versus cell rigidity for RBCs of two different sizes, $D_{\rm rbc} = 6, 8\,\mu$m. (c) Pe_λ versus feeding hematocrit $H_{\rm F}$, also for RBCs of $D_{\rm rbc} = 6, 8\,\mu$m.

Besides the curvature of the stagnation point at the apex, other factors can also affect the interaction between the cells and the bifurcation, leading to either weakened or enhanced RBC lingering. Taking the bifurcation in Fig. 2a for example (Fig. 7a), three physiologically-relevant aspects are explored:

the cell size D_{RBC} , the cell rigidity κ_{s} and the feeding Hematocrit H_{F}. As shown in Fig. 7$b-c$, the smaller cells simulated ($D_{\mathrm{RBC}} = 6\mu$m, matching normal mouse RBC size) in general experience more intense lingering than the larger ones, which are modelled through increasing the cell diameter to $D_{\mathrm{RBC}} = 8\mu$m while maintaining the same H_{F}. In other words, increasing the level of cell-confinement at the capillary level reduces the possibility of RBC lingering.

Increased cell rigidity (imitating diseased RBCs with higher-level stiffness) is found to introduce strong cell-wall and cell-cell steric repulsion at the bifurcation apex (see enlarged gaps near the branching point as shown in Fig. 7a), thus reducing the overall lingering frequency or duration of individual lingering events as indicated by a smaller Pe_λ (Fig. 7b). On the other hand, for identical flow conditions, enriched hematocrit ($H_{\mathrm{F}} = 33\%$) in the mother branch has a weakening effect on RBC lingering at the bifurcation whereas reduced hematocrit ($H_{\mathrm{F}} = 10\%$) has a strengthening effect compared to the experimentally measured value $H_{\mathrm{F}} = 26\%$ for this bifurcation (Fig. 7c). The probable reason behind the decreased Pe_λ in this case is that crowded cell traffic reduces the possibility of individual RBCs residing on the apex for extended periods of time as they are more likely to be pushed forward by following cells.

Conclusion

Our study demonstrates that lingering (i.e. RBCs temporarily residing near the bifurcation apex with diminished velocity) is a mechanism, which can significantly modify the partitioning of red blood cells (RBCs) through bifurcations. Therefore, it should be taken into account when predicting the hematocrit distribution in microvascular networks at the capillary level.

Existing literature has extensively tested and validated the Zweifach-Fung effect in microvascular bifurcations at the arteriolar level, mostly through microfluidic experiments or numerical simulations. Nonetheless, studies that focus on the mere effect of RBC-bifurcation interaction are rare and it remains largely unknown how well the Pries-Secomb model describes the RBC partitioning at the highly-confined capillary level in vivo, where the cells need to squeeze through vessels and the cell-free layer (a key constituent in the empirical model of Pries et al.) is negligible. Previous numerical-experimental works suggested that the branching geometry and cross-sections of the daughter branches can bias the partitioning of capsules at a bifurcation, depending on the size and deformability of the capsule [33]. With much higher confinement reflecting the capillary blood flow, our study represents the first in vivo demonstration of the effect of bifurcation geometry and cell properties, and provides a mechanistic justification through the microscopic cell-wall interaction, namely lingering, on the partitioning of RBCs.

Furthermore, we have shown that lingering introduces some degree of asymmetry between the daughter branches (Fig. 5), which can either reinforce the Zweifach-Fung effect, or revert it. Indeed, Supplemental Figure S6 illustrates that both positive and negative deviations from the Pries model can be observed at a high lingering Péclet number. A similar trend is observed for deviations from the linear scaling (for which the fractional erythrocyte flow rate is equal to the fractional blood flow rate $FQ_e = FQ_b$, see Supp. Fig. S6). The key finding is that the lingering phenomenon is a prevalent mechanism in the capillary bed, subject to the fractional flows and local geometry of the bifurcation. We demonstrate that, under the assumption of plug flow given highly-confined cell motion, the lingering Péclet number (Pe_λ) correlates with the flow rate ratio Q_{SD}/Q_{MD}. The subscripts MD and SD refer to the Main Daughter and Secondary Daughter, respectively. This ratio Q_{SD}/Q_{MD} determines the position of the stagnation point, where the local curvature is further found correlated with the lingering intensity.

Our findings on the modulating effect of RBCs lingering on hematocrit distribution have important implications for remodeling of the microvascular network occurring in development or reintroduced in disease. Recently, it has been uncovered that RBC distribution is strongly associated with the pattern of vascular remodeling, presumably by affecting the wall shear stress difference in neighbouring branches through effective blood viscosity [14]. Since lingering can substantially influence the RBC partitioning at capillary bifurcations (in extreme cases revert it), one can expect that lingering may play a key role in shaping the microcirculatory network. Additionally, since the deformability of RBCs affects their characteristic lingering time and, consequently, their partitioning, lingering might be a route through which the microvascular blood flow is impaired in diseases involving hardening of RBCs [20, 21, 22, 23, 24, 25]. Further in vivo investigations with rigidified RBCs should be performed in

future work to test this hypothesis experimentally.

Finally, this work highlights the need for more models dedicated to RBC studies considering high confinement, as observed in microcirculatory environments entailing the lingering phenomena. Our results highlight the importance of input parameters, such as the flow split in the bifurcation and the curvature of the apex region of the bifurcation.

Author Contributions

AD, CW, MWL, LK and MDM designed the research. GS, MWL and MDM designed, planned and obtained authorizations for animal experiments. GS and MWL performed the surgery and recorded the movies. YR, AD, AK, MB and TJ designed, wrote and maintained the experimental movie analysis methods. QZ designed the simulation and performed the numerical analysis with input from TK and MOB. YR, AD and QZ wrote the manuscript. All authors discussed the results and critically reviewed the article.

Acknowledgments

This work was supported by the research unit FOR 2688 - Wa1336/12 and LA2682/9-1 of the German Research Foundation, and by the Marie Skłodowska-Curie grant agreement No. 860436—EVIDENCE. A.D. acknowledges funding by the Young Investigator Grant of the Saarland University.

References

[1] Y C Fung and B W Zweifach. Microcirculation: Mechanics of Blood Flow in Capillaries. *Annu. Rev. Fluid Mech.*, 3(1):189–210, jan 1971.

[2] AR Pries, K Ley, and P Gaehtgens. Generalization of the fahraeus principle for microvessel networks. *American Journal of Physiology-Heart and Circulatory Physiology*, 251(6):H1324–H1332, 1986.

[3] Alexander Farutin and Chaouqi Misbah. Symmetry breaking and cross-streamline migration of three-dimensional vesicles in an axial poiseuille flow. *Physical review E*, 89(4):042709, 2014.

[4] E. Kaliviotis, J. M. Sherwood, and S. Balabani. Partitioning of red blood cell aggregates in bifurcating microscale flows. *Sci. Rep.*, 7(1):44563, apr 2017.

[5] E. Kaliviotis, J. M. Sherwood, and S. Balabani. Local viscosity distribution in bifurcating microfluidic blood flows. *Phys. Fluids*, 30(3):030706, mar 2018.

[6] A. Mantegazza, F. Clavica, and D. Obrist. In vitro investigations of red blood cell phase separation in a complex microchannel network. *Biomicrofluidics*, 14(1):014101, jan 2020.

[7] Zaiyi Shen, Gwennou Coupier, Badr Kaoui, Benoît Polack, Jens Harting, Chaouqi Misbah, and Thomas Podgorski. Inversion of hematocrit partition at microfluidic bifurcations. *Microvasc. Res.*, 105:40–46, may 2016.

[8] Andrew Pskowski, Prosenjit Bagchi, and Jeffrey D Zahn. Investigation of red blood cell partitioning in an in vitro microvascular bifurcation. *Artificial organs*, 45(9):1083–1096, 2021.

[9] A.R. Pries, K. Ley, M. Claassen, and P. Gaehtgens. Red cell distribution at microvascular bifurcations. *Microvasc. Res.*, 38(1):81–101, jul 1989.

[10] Axel R Pries, Timothy W Secomb, P Gaehtgens, and JF Gross. Blood flow in microvascular networks. experiments and simulation. *Circulation research*, 67(4):826–834, 1990.

[11] Axel R Pries, Bettina Reglin, and Timothy W Secomb. Structural response of microcirculatory networks to changes in demand: information transfer by shear stress. *American Journal of Physiology-Heart and Circulatory Physiology*, 284(6):H2204–H2212, 2003.

[12] Zixiang L Liu, Jonathan R Clausen, Justin L Wagner, Kimberly S Butler, Dan S Bolintineanu, Jeremy B Lechman, Rekha R Rao, and Cyrus K Aidun. Heterogeneous partition of cellular blood-borne nanoparticles through microvascular bifurcations. *Physical Review E*, 102(1):013310, 2020.

[13] Qi Zhou, Joana Fidalgo, Miguel O Bernabeu, Mónica SN Oliveira, and Timm Krüger. Emergent cell-free layer asymmetry and biased haematocrit partition in a biomimetic vascular network of successive bifurcations. *Soft Matter*, 17(13):3619–3633, 2021.

[14] Qi Zhou, Tijana Perovic, Ines Fechner, Lowell T Edgar, Peter R Hoskins, Holger Gerhardt, Timm Krüger, and Miguel O Bernabeu. Association between erythrocyte dynamics and vessel remodelling in developmental vascular networks. *Journal of the Royal Society Interface*, 18(179):20210113, 2021.

[15] Peter Balogh and Prosenjit Bagchi. Analysis of red blood cell partitioning at bifurcations in simulated microvascular networks. *Physics of Fluids*, 30(5):051902, 2018.

[16] Shyr-Shea Chang, Shenyinying Tu, Kyung In Baek, Andrew Pietersen, Yu-Hsiu Liu, Van M Savage, Sheng-Ping L Hwang, Tzung K Hsiai, and Marcus Roper. Optimal occlusion uniformly partitions red blood cells fluxes within a microvascular network. *PLoS computational biology*, 13(12):e1005892, 2017.

[17] Jared O Barber, Jonathan P Alberding, Juan M Restrepo, and Timothy W Secomb. Simulated two-dimensional red blood cell motion, deformation, and partitioning in microvessel bifurcations. *Annals of biomedical engineering*, 36(10):1690–1698, 2008.

[18] Peter Balogh and Prosenjit Bagchi. Direct numerical simulation of cellular-scale blood flow in 3d microvascular networks. *Biophysical journal*, 113(12):2815–2826, 2017.

[19] Alexander Kihm, Stephan Quint, Matthias W Laschke, Michael D Menger, Thomas John, Lars Kaestner, and Christian Wagner. Lingering dynamics in microvascular blood flow. *Biophysical Journal*, 120(3):432–439, 2021.

[20] J. Stuart and G.B. Nash. Red cell deformability and haematological disorders. *Blood Rev.*, 4(3):141–147, sep 1990.

[21] A.M. Dondorp, M. Nyanoti, P.A. Kager, S. Mithwani, J. Vreeken, and K. Marsh. The role of reduced red cell deformability in the pathogenesis of severe falciparum malaria and its restoration by blood transfusion. *Trans. R. Soc. Trop. Med. Hyg.*, 96(3):282–286, may 2002.

[22] A. Symeonidis, G. Athanassiou, A. Psiroyannis, V. Kyriazopoulou, K. Kapatais-Zoumbos, Y. Missirlis, and N. Zoumbos. Impairment of erythrocyte viscoelasticity is correlated with levels of glycosylated haemoglobin in diabetic patients. *Clin. Lab. Haematol.*, 23(2):103–109, apr 2001.

[23] Robert Mannino, David R Myers, Yumiko Sakurai, Russell E. Ware, Gilda Barabino, and Wilbur Lam. Increased Erythrocyte Rigidity Is Sufficient to Cause Endothelial Dysfunction in Sickle Cell Disease. *Blood*, 120(21):818–818, nov 2012.

[24] Felix Reichel, Martin Kräter, Kevin Peikert, Hannes Glaß, Philipp Rosendahl, Maik Herbig, Alejandro Rivera Prieto, Alexander Kihm, Giel Bosman, Lars Kaestner, Andreas Hermann, and Jochen Guck. Changes in Blood Cell Deformability in Chorea-Acanthocytosis and Effects of Treatment With Dasatinib or Lithium. *Front. Physiol.*, 13(April):1–11, apr 2022.

[25] Antonia Rabe, Alexander Kihm, Alexis Darras, Kevin Peikert, Greta Simionato, Anil Kumar Dasanna, Hannes Glaß, Jürgen Geisel, Stephan Quint, Adrian Danek, Christian Wagner, Dmitry A. Fedosov, Andreas Hermann, and Lars Kaestner. The Erythrocyte Sedimentation Rate and Its Relation to Cell Shape and Rigidity of Red Blood Cells from Chorea-Acanthocytosis Patients in an Off-Label Treatment with Dasatinib. *Biomolecules*, 11(5):727, may 2021.

[26] Matthias W Laschke, Brigitte Vollmar, and Michael D Menger. The dorsal skinfold chamber: window into the dynamic interaction of biomaterials with their surrounding host tissue. *Eur Cell Mater*, 22(147):e64, 2011.

[27] Xiangyang Xu, Shengzhou Xu, Lianghai Jin, and Enmin Song. Characteristic analysis of otsu threshold and its applications. *Pattern recognition letters*, 32(7):956–961, 2011.

[28] Ivo F Sbalzarini and Petros Koumoutsakos. Feature point tracking and trajectory analysis for video imaging in cell biology. *Journal of structural biology*, 151(2):182–195, 2005.

[29] Miguel O Bernabeu, Martin L Jones, Rupert W Nash, Anna Pezzarossa, Peter V Coveney, Holger Gerhardt, and Claudio A Franco. Polnet: A tool to quantify network-level cell polarity and blood flow in vascular remodeling. *Biophysical journal*, 114(9):2052–2058, 2018.

[30] AR Pries, K Ley, M Claassen, and P Gaehtgens. Red cell distribution at microvascular bifurcations. *Microvascular research*, 38(1):81–101, 1989.

[31] Yasuhiko Sugii, Remi Okuda, Koji Okamoto, and Haruki Madarame. Velocity measurement of both red blood cells and plasma of in vitro blood flow using high-speed micro piv technique. *Measurement science and Technology*, 16(5):1126, 2005.

[32] S Chien, CHRISTIAN D Tvetenstrand, MA Epstein, and GEERT W Schmid-Schonbein. Model studies on distributions of blood cells at microvascular bifurcations. *American Journal of Physiology-Heart and Circulatory Physiology*, 248(4):H568–H576, 1985.

[33] Z Wang, Y Sui, A-V Salsac, D Barthès-Biesel, and W Wang. Path selection of a spherical capsule in a microfluidic branched channel: Towards the design of an enrichment device. *Journal of Fluid Mechanics*, 849:136–162, 2018.